ACS OMEGA

Open Access



http://pubs.acs.org/journal/acsodf

Article

# Oyster Shell Powder/PCL Composite Scaffolds Loaded with Psoralen Nanospheres Promote Large Bone Defect Repair

Tianpeng Liu,[#] Menghan Chen,[#] Yifan Zhao, Shaochuan Zhao, Chen Rui, Wenxiong Li,* and Feng Yang*

Cite This: *ACS Omega* 2025, 10, 2231−2242

Read Online

ACCESS | Metrics & More | Article Recommendations

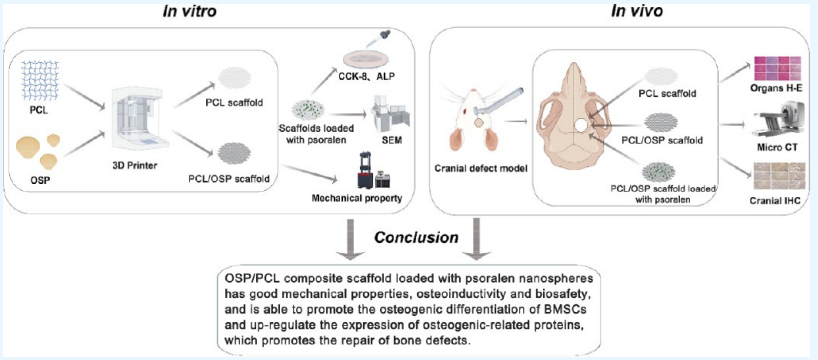


**ABSTRACT:** Research on bone substitutes for repairing bone defects has drawn increasing attention, and the efficacy of three-dimensional (3D) printed bioactive porous scaffolds for bone defect repair has been well documented. Our previous studies have shown that psoralen can promote osteogenesis by activating the Wnt/$\beta$-catenin and BMP/Smad signaling pathways and their crosstalk effects, and psoralen nanospheres have a good osteogenesis-promoting effect *in vitro* with low cytotoxicity. The Chinese medicine oyster shell powder, characterized by its porous structure, strong adsorption, and unique bioactivity, has potential in fracture-promoting repair materials. However, the effect of loading psoralen nanospheres onto oyster shell powder/polycaprolactone (OSP/PCL) scaffolds to repair bone defects is unclear. In this study, composite scaffolds consisting of OSP PCL were prepared by 3D printing, and psoralen nanospheres were adhered to the scaffolds. The characterization features of the composite scaffold system were investigated *in vitro* concerning the biocompatibility of bone mesenchymal stem cells (BMSCs). The efficacy of the composite scaffolds for repairing bone defects was explored *in vivo* through a rat cranial bone defect model. The results showed that the composite scaffolds were homogeneous porous structures with high mechanical strength and could be adhered well by the psoralen-loaded nanospheres. *In vitro* studies showed that the scaffolds had good biocompatibility with BMSCs and positively affected the expression of osteogenic differentiation-related proteins. *In vivo* studies showed that the composite scaffolds could more effectively promote the formation of new bone in the defect area (Φ5 mm) compared to the pure PCL scaffolds. At the same time, the composite scaffolds containing psoralen had a more significant stimulating effect on the healing of the cranial defects compared with the OSP/PCL scaffolds without psoralen.

## 1. INTRODUCTION

Large segmental bone defects caused by trauma, infection, osteoporosis, and other bone metabolism diseases have been a major clinical challenge in orthopedics. The bone itself can regenerate, and no significant interventions are needed for small-scale bone injuries. Still, for defects larger than the critical size, the regenerative capacity of bone tissue is not enough to heal itself, and surgical treatment is usually required.[1−3] Conventional surgical treatment of bone defects is associated with long, arduous, and often multiple surgeries, which places a tremendous psychological and financial burden on the patient. Therefore, the search for an effective treatment modality that can reduce the burden on the patient has become an urgent problem.

Bone tissue engineering (BTE) is usually known for using high-density BMSCs as seed cells, inoculating them in an extracellular matrix with good biocompatibility, then trans-

Received: October 9, 2024
Revised: December 13, 2024
Accepted: December 17, 2024
Published: January 9, 2025

planting them into bone defects to achieve continuous proliferation and degradation of osteoblasts, and ultimately leading to the repair of bone defects.[4] This technique can not only repair large bone defects but also can be shaped on demand and mass-produced, which overcomes the shortcomings of autologous and allogeneic bone grafts in terms of damage to the donor area, immune rejection, and pathogenicity and is an ideal technique for the repair of large bone defects.[5]

Some natural biomaterials in traditional Chinese medicine strengthen the bone, and their use in bone tissue engineering scaffold materials has specific feasibility and scientific validity.[6] The porous structure, outstanding specific surface area, and excellent adsorption properties of oyster shells in traditional Chinese medicine make them effective against bacteria such as Escherichia coliand *Staphylococcus aureus*.[7] In addition, oyster shells possess potent bioactivities, which are particularly prominent in improving bone structure and function.[8] According to Mount et al.,[9] there is an excellent correlation between the formation of oyster shells and calcium deposition in humans, so oyster shells can be used as a high-quality bone tissue repair material. Pharmacological research studies have shown that the traditional Chinese medicine tonic fat has various properties such as vasodilator, antitumor, antibacterial, and anticytotoxic.[10] In addition, psoralen, the monomer of psoralen, can activate osteoblasts through signaling pathways such as ERK and BMP, induce osteogenic differentiation, increase the number of osteoblasts in fracture callus, and accelerate fracture healing.[11,12]

Polycaprolactone (PCL) is an organic polymer that can be used as a raw material for a variety of biomaterials[13] and has the advantage of biocompatibility to avoid severe inflammatory reactions, in addition to its relatively low melting temperature and excellent thermal stability at a low price.[14,15] However, there are not enough studies on the application of PCL-based composites for bone tissue engineering.[16]

Our previous studies have demonstrated that psoralen can regulate the osteogenic differentiation of BMSCs through the Wnt/$\beta$-catenin and BMP/Smad signaling pathways and play a promotional role in the osteogenic differentiation of BMSCs.[17,18] Therefore, in this study, psoralen was prepared as psoralen nanospheres by solvent evaporation and then adhered to the surface of oyster shell powder/PCL scaffolds by collagen coating to evaluate the characterization of the psoralen-loaded nanosphere composite 3D-printed PCL/oyster shell powder (PCL/OSP) scaffolds and their biocompatibility with bone marrow mesenchymal stem cells (BMSCs) and to evaluate the composite scaffold system's capability of repairing bone defects *in vivo* by using a rat cranial bone defect model.

## 2. MATERIALS AND METHODS

**2.1. Preparation of Psoralen-Loaded Nanospheres.** The solvent evaporation method was used to prepare nanospheres loaded with psoralen: 25 mg of tonicin (MCE, USA) and 125 mg of PLGA (MCE, USA) were weighed precisely, dissolved in 5 mL of dichloromethane (Sigma-Aldrich, USA) and 0.5 mL of purified water, then emulsified by ultrasonic emulsification for 3 min, and pulverized by an ultrasonic pulverizer (Shanghai Weimi Technology Co., Ltd., China) for 5 min to form colostrum. Then the colostrum was added to 7 mL of 1% PVA, pulverized by an ultrasonic pulverizer for 4 min, and then poured into 120 mL of 0.2% PVA (Shandong Yousuo Chemical Technology Co., Ltd., China) solution and stirred at 37 °C using a magnetic stirrer (Thermo, USA) at a speed of 3000 rpm for 4 h to evaporate the organic solvent. Then the nanospheres were centrifuged at 1000 rpm for 10 min using a centrifuge (IKA, Germany), the nanosphere precipitates were washed three times with pure water, and then the nanospheres were frozen in a refrigerator at −80 °C for 30 min and then put into a freeze-dryer (Ningbo Scientz Biotechnology Co., Ltd., China) for 24 h to prepare the psoralen nanometer nanosphere dry powder.

**2.2. Fabrication of Composite 3D Scaffolds.** The oyster shells used in this experiment were purchased from the Affiliated Hospital of Shaanxi University of Traditional Chinese Medicine. The School of Mechanical Engineering, Xi'an Jiaotong University prepared the PCL and the OSP/PCL composite 3D scaffolds. (i) Preparation of PCL−oyster shell powder printing material: PCL (medical grade, 80,000 molecular weight, purchased from Solvay, USA) and glacial acetic acid (Sigma-Aldrich, USA) were added into a reagent bottle at a 1:3 mass/volume ratio. A magnetic stirrer was placed in the reagent vial, and the vial was placed on a magnetic stirrer until PCL was completely dissolved. Oyster shell powder was added to the PCL acetic acid solution at 3%, 4%, 5%, 6%, and 7% of the mass ratio of oyster shell powder/polycaprolactone and stirred overnight until the oyster shell powder was well dispersed to obtain the polycaprolactone oyster shell powder acetic acid solution at each mass ratio. The PCL and oyster shell powder acetic acid solution was poured into a Petri dish (Hong Kong XABC Biotech Co., Ltd.) and placed in a fume hood to dry for 5 days until the acetic acid completely evaporated to obtain a thin film of PCL−oyster shell powder printing material. (ii) Printing of oyster shell powder/PCL scaffolds: using a bioprinter (Shaanxi Baipusheng Medical Technology Development Co., Ltd., China), thin-film PCL−oyster shell powder was cut into small pieces and loaded into a 2.5 mL glass microsampler, and a stainless steel dispensing needle with an inner diameter of 0.2 mm was installed at the top of the sampler. A stainless steel dispensing needle was installed at the top of the injector. The microsampler was placed in the electrostatic printing nozzle of the bio-3D printer, and the pneumatic extrusion pressure connector was inserted at the end. A glass sheet was placed on the receiving platform of the bio-3D printer as a printing substrate. The scaffold printing parameters were as follows: printing speed: 1.5 mm/s, extrusion pressure: 1900 mbar, scaffold layer height: 0.2 mm, scaffold line spacing: 0.8 nm, and the number of scaffold layers: 4 layers. After printing, the scaffold was removed from the glass sheet and placed in 75% alcohol for sterilization. (iii) PCL scaffolds were prepared as described above.

**2.3. Characterization Observations of Composite 3D Scaffolds.** *2.3.1. Morphological Observation and Porosity Determination.* The surface morphology of the different scaffolds was observed separately after spraying the scaffolds with gold under a vacuum using a field emission scanning electron microscope (SEM) (TESCAN, Czech Republic). The weighing method was used: porosity was calculated according to the mass of the perforated scaffold compared to the solid scaffold: $\rho = m_1/m_2$, $m_1$ is the weight of the perforated scaffold, and $m_2$ is the weight of the solid scaffold.

*2.3.2. Mechanical Performance Test.* The 5% oyster shell powder/PCL scaffolds and pure PCL scaffolds ($n$ = 4) were randomly taken to test their modulus of elasticity using a



https://doi.org/10.1021/acsomega.4c09221
ACS Omega 2025, 10, 2231−2242

universal mechanical testing machine (Guangdong Baoda Xuanli Technology Co., Ltd., China), and the optimal loading module was precisely selected according to the operation guide. The loading rate was 0.1 mm/min at room temperature. The compression tests were conducted on four samples in each group. According to mechanical theory, the compressive elastic modulus of the material is found from the stress/strain. Here, stress = $P/A$ and strain = $h/L$. $P$ is the load, $A$ is the material cross-sectional area, $h$ is the compression length, and $L$ is the initial length of the sample. By organizing the data, we could calculate the stress and strain separately and draw a stress−strain graph. We could intercept the deformation in a more fixed section of the straight-line region in the linear range and use its slope as the material's elastic modulus.

*2.3.3. Observation of Micronanosphere Adhesion to Scaffolds.* In this study, collagen was used as a medium for the adhesion of psoralen nanospheres to the surface of porous composite scaffolds so that the composite scaffolds could gradually release psoralen to promote the growth of cells inside the scaffolds, and the adhesion was carried out in the following two steps:

Preparation of collagen-coated composite scaffolds: Type I collagen was fully dissolved in 0.05 M acetic acid solution (Solarbio, China), and then the pH was adjusted to neutral with NaOH solution, followed by 2-morpholinoethanesulfonic acid buffer (2-(4-morpholino) ethanesulfonic acid, MES) (Beyotime, China) to regulate the collagen solution concentration to 0.1 g/mL. Finally, the scaffolds were immersed in it for 2 h. 1-(3-(Dimethylamino)propyl)-3-ethylcarbodiimide hydrochloride (EDC) (Shanghai Macklin Biochemical Co., Ltd., China) and *N*-hydroxysuccinimide (NHS) (Shanghai Macklin Biochemical Co., Ltd., China) dissolved in MES were added to the above collagen solution so that the final concentration of EDC was 2.5 mg/mL. The final concentration of NHS was 0.63 mg/mL, and the collagen was cross-linked continuously for 4 h. On this basis, the collagen-adsorbed scaffolds were removed, vacuum-dried at room temperature for 24 h, gently washed twice with phosphate buffered saline (PBS), freeze-dried for 24 h at room temperature using a freeze-dryer (Ningbo Scientz Biotechnology Co., Ltd., China), and then frozen and stored in a refrigerator at −20 °C.

Preparation of psoralen nanosphere scaffolds: The nano-nanospheres were complexed with collagen by the stepwise incorporation method, and a collagen membrane was prepared on their surface by the (i) method. The nanospheres were mixed with deionized water to make a mixture of 50 mg/mL and shaken well to obtain the suspension of psoralen nanoparticles. The support was placed in a 24-well plate (Hong Kong XABC Biotech Co., Ltd.), and 50 μL of nanosphere suspension was gently dripped onto the collagen-coated scaffolds, vacuum-dried at room temperature for 24 h, and stored at −20 °C. After the preparation of nano-nanosphere-adherent composite scaffolds, they were characterized and detected by scanning electron microscopy. Gold powder was sputtered onto the prepared composite scaffolds, and the surface morphology was observed by scanning electron microscopy.

**2.4. Biocompatibility Testing of Composite Scaffolds with BMSCs.** The scaffolds were categorized into (a) PCL group: pure PCL scaffolds, (b) 5%OSP/PCL group: PCL scaffolds containing 5%OSP, and (c) psoralen + 5%OSP/95% PCL group: psoralen-loaded scaffolds containing 5% oyster shell powder/PCL. Then the scaffolds were cultured in composite with the third-generation BMSCs in the following steps:

Sterilization of the scaffold: Wash the scaffold with pure water 3 times for 10 min/time, put it in 75% alcohol for 30 min, wash it with sterile PBS (Boster Biological Technology Co., Ltd., China) 3 times for 10 min/time, irradiate it with ultraviolet radiation for 1 h, and store it for future use. The above steps were operated on a sterile ultraclean table.

Preparation of the scaffolds and cell composite culture: Take the scaffolds and place them in 24-well plates. Add 2 mL of DMEM culture solution (Cytiva, Australia) containing 10% fetal bovine serum (Gibco, Australia) to each well, submerge, and coat the scaffolds, so that the medium is fully immersed in the scaffolds, and place them into the cell culture incubator (Esco Micro Pte. Ltd., Singapore) to be prewetted for 24 h.

Scaffold and cell culture: After 24 h, prepare a new 24-well plate with a layer of agarose in advance, take out the scaffold soaked in culture medium, and place it on the new 24-well plate. Add 1 mL of third-generation BMSCs with a cell density of $1 \times 10^5$/mL per well (from Shanghai Zhong Qiao Xin Zhou Biotechnology Co., Ltd., China), incubate at 37 °C, 5% $CO_2$ by volume and saturated humidity incubator for 30 min, and then gently shake the plate twice every 15 min. After the cells adhered to the wall, 1 mL per well was added with 10% fetal bovine serum, 1% double antibody (Cytiva, Australia), and 1% glutamine (BOSTER Biological Technology Co., Ltd., China) DMEM medium to average volume and placed in the incubator to continue the complex culture, using the half-exchange method once every 2−3 days, each time the amount of fluid change is 1/2−2/3 of the original culture medium; an inverted phase contrast microscope (Nexcope, USA) was used to observe the adsorption of the cells and the scaffold.

*2.4.1. CCK-8 Assay for Cell Proliferative Activity.* On the first, fourth, and seventh day of cell-scaffold coculture, the cell-scaffold-compliant culture system was tested by CCK-8 (Cell Counting Kit-8) (Bioss, China). In a 24-well plate, three replicate wells were set up in each group, 500 μL of fresh medium was added to each well, and 50 μL of CCK-8 solution was added to each well (medium:CCK reagent = 10:1), and after incubation for 2 h in a constant temperature incubator, 100 μL of culture solution from the 24-well plate was inhaled into a new 96-well plate. Absorbance values at 450 nm were measured by an enzyme labeling instrument (Biotek, USA) to reflect the cell viability indirectly. The absorbance value at 450 nm indirectly reflects the number of live cells.

*2.4.2. Cell Viability Assay.* In 24-well plates, BMSCs in the quantity of $5 \times 10^4$/well were inoculated onto the surface of the scaffolds in groups (a), (b), and (c), respectively, and the growth of the cells on the scaffolds was detected by using the Live/Dead Cell Staining Kit (Beyotime, China) after 3 days of incubation in an incubator. The steps of the cell live-dead experiment are as follows: (i) thaw the Calcein-AM and PI stock solution at room temperature for 0.5 h before use.


https://doi.org/10.1021/acsomega.4c09221
ACS Omega 2025, 10, 2231−2242

Prepare 1 mL of buffer, add 2 μL of Calcein-AM stock solution and 4 μL of PI stock solution, and mix as a working solution. (ii) Rinse the holder with PBS first, then inject the working solution into the wells to be tested. (iii) Wrap the 96-well plate in aluminum foil and place it in a light-proof box; keep at 37 °C for 0.5 h. (iv) Each well was rinsed three times so that the fluorescent reagent was rinsed cleanly on the holder for easy observation. The samples were placed under a laser confocal microscope and examined for live cells (yellow-green fluorescence) and dead cells (red fluorescence) by using a 490 nm excitation filter.

*2.4.3. Effect of Composite Scaffolds on the Osteogenic Capacity of BMSCs.* BMSCs were inoculated in 24-well plates at $6 \times 10^3$/well and incubated at 37 °C and 5% $CO_2$ in an incubator. After the BMSCs adhered to the well plates, each group was switched to a culture with an osteogenic induction medium. ALP staining was performed after the fourth day of incubation with each group of scaffolds separately to evaluate its effect on the early osteogenic differentiation ability of BMSCs, and the staining was performed with an alkaline phosphatase staining kit as follows: (i) mix the incubation solution A (ALP fixation solution) and solution B (a mixed solution of AS-BI buffer and fast blue B stain) as the incubation working solution before use. (ii) The medium in the well plate was aspirated and discarded, rinsed three times with PBS, and fixed with 70% alcohol, and the fixative was washed off with distilled water. (iii) Add incubation working solution to cover the samples for 180 min at 37 °C. Wash with water for 5−10 min (Note: Negative control is selected to be incubated with negative control solution for 3 h, and other operations are the same as those of the normal group). (iv) Staining solution A covered the samples with incubation at room temperature for 5 min and washed them with water for 2 min. (v) Staining solution B covered the samples with incubation at room temperature for 1 min and washed with water for 5 min. A microscope then observed the staining. Meanwhile, alkaline phosphatase activity was measured using an alkaline phosphatase colorimetric assay kit for each group of scaffolds on days 4 and 7 of coculture and quantified according to protein concentration.

*2.4.4. Observation of the Adhesion State of BMSCs to Composite Scaffolds.* On the fourth day of complex culture in 24-well plates, the cell scaffold complexes of the three groups, blank, oyster shell powder, and experimental, were observed by scanning electron microscopy to assess the adhesion level. They were first rinsed twice with PBS, then immersed in 4% glutaraldehyde solution, and fixed at 4 °C for 2 h. Finally, the fixative was aspirated with a pipet gun, washed again twice with PBS, and then dehydrated in graded ethanol solutions with volume fractions of 50%, 70%, 80%, 90%, and 100% in sequence, with each gradient lasting for 10 min; after drying at room temperature, the samples were gently adhered to conductive adhesives on the samples, then metal plated by a vacuum spray plating technique, and finally observed by electron microscopy.

**2.5. Evaluation of the Efficacy of Composite Scaffolds for Repairing Cranial Defects in Rats.** *2.5.1. Establishment of a Rat Cranial Defect Model and Implantation of Composite Scaffolds.* The cranial defect model was prepared based on the modeling method of Mohan and other scholars.[19] Each rat was weighed and anesthetized by intraperitoneal injection using 10% chloral hydrate (0.4 mL/100 g) (Tianjin Damao Chemical Reagent Co., Ltd.), the skin was prepared and then disinfected and toweled at the parietal bone site, a 2 cm sagittal incision was made, and the subcutaneous skin tissues and periosteum were cut in order to reach the bone surface, exposing the cranial bone surface. A bone extraction drill was used to prepare the cranial bone defect model. A full-layer bone defect with a diameter of $d$ = 5 mm was prepared in the parietal bone of the rat using an osteotomized drill (note that saline was sprinkled to cool the temperature when drilling the skull to prevent the brain tissue of the rat from being injured by the high local temperature). A full-layer defect was formed in the cranial bone. The experimental animals were randomly grouped (10 animals/group) as follows: (a) blank group: pure PCL scaffolds (PCL scaffolds); (b) scaffolds without psoralen: oyster shell powder/PCL scaffolds containing 5% oyster shell powder/PCL scaffolds (5%OSP/PCL scaffolds); and (c) scaffolds containing psoralen: 5%OSP/PCL scaffolds containing psoralen (psoralen + 5%OSP/PCL scaffolds). Different scaffold materials were implanted according to the experimental groups, and the wound was closed tightly in layers. After the operation, 200,000 U/100 g of penicillin (Harbin Pharmaceutical Group Co., Ltd., China) was injected intramuscularly, and erythromycin ointment (Chongqing Kerui Pharmaceutical (Group) Co., Ltd.) was applied locally on the wounds every day for 7 days to prevent infection. This experiment was approved by the Laboratory Animal Ethics Committee of Shaanxi University of Traditional Chinese Medicine (Ethics Approval number SUCMDL20221116002).

*2.5.2. Composite Scaffold In Vivo Toxicity Testing.* In the second week postoperatively, two rats from each group were taken and overdosed with 4% chloral hydrate. Then, their livers, kidneys, spleens, and hearts were fixed in 4% paraformaldehyde (Wuhan Servicebio Technology Co., Ltd.) for 24 h. Then, gradient dehydration was performed using ethanol and rotary slicers (Leica, Germany) to prepare paraffin-embedded sections (thickness = 4 μm). Finally, hematoxylin−eosin staining boxes (H−E) (Beijing Leagene) were used. The paraffin-embedded sections (thickness = 4 μm) were stained with hematoxylin−eosin staining (H−E) (Beijing League Biotech. Co., Ltd., China). Finally, the histological morphology of the above organs was observed by using an ordinary light microscope.

*2.5.3. Micro CT Detection of Bone Regeneration in Bone Defects.* The following metrics were measured: bone volume fraction (BV/TV) = volume of newly formed bone/total volume of region of interest (ROI), trabecular Number (Tb.N), trabecular thickness, Tb.Th), and trabecular spacing (Tb.Sp) to understand the mass of newly formed bone and trabecular strength. Trabecular number (Tb.N), trabecular thickness (Tb.Th), and trabecular separation (Tb.Sp) were measured in order to understand the quality of the newly formed bone and the strength of the trabeculae. At the end of the examination, cranial specimens were taken and fixed in 4% paraformaldehyde for backup.

*2.5.4. Histologic Analysis of New Bone at Bone Defects.* Cranial specimens were taken at 0.5 cm around the bone defect area after 24 h of fixation in 4% paraformaldehyde. Paraffin sections were made after 4 weeks of decalcification. Immunohistochemistry was carried out using the SABC (Strept Avidin−Biotin Complex) method (Boster Biological Technology Co., Ltd, China) to detect the expression levels of ALP, osteoprotegerin (OPG), and BMP-2. Paraffin sections were dewaxed to water, incubated with 3% hydrogen peroxide


https://doi.org/10.1021/acsomega.4c09221
ACS Omega 2025, 10, 2231−2242

solution for 5 min at room temperature to eliminate endogenous peroxidase activity, and rinsed with PBS for 5 min ×3 times. Sections were antigenically repaired by using thermal repair. Drops were incubated with 5% BSA blocking solution at 37 °C for 0.5 h and then shaken dry without rinsing, and diluted primary antibody was added and refrigerated at 4 °C overnight. The sections were removed from the refrigerator, rewarmed for 0.5 h, rinsed in PBS for 5 min ×3 times, incubated dropwise with secondary antibody at 37 °C for 0.5 h, and rinsed in PBS for 5 min ×3 times. SABC solution was added dropwise, incubated at 37 °C for 0.5 h, and rinsed with PBS for 5 min ×3 times. The DAB chromogenic solution was added dropwise to the sectioned tissues. After the sections turned brownish yellow, the color development was stopped by rinsing with tap water, the nuclei were restained with hematoxylin and then dehydrated and sealed, and the images were observed and collected for analysis with an ordinary optical microscope. No less than three 200× field-of-view photographs were taken in each section so that the tissues filled the whole field of view as much as possible and the background color of each image was kept the same. ImageJ software version 1.8.0 (NIH, USA) was used to select the same brown color as a uniform criterion for determining the positive determination, and each photograph was counted to calculate the positive cumulative optical density value (IOD) and the area of the tissue image element (AREA). The average optical density (AO) was calculated, AO = IOD/AREA; the larger the AO value, the higher the positive expression of this protein.

**2.6. Statistical Analysis.** SPSS 25.0 (IBM Software, USA), GraphPad Prism 10 (GraphPad Software, USA), and Adobe Illustrator 2021 (Adobe, USA) software were selected for data analysis and graphing. The results of the experiments were expressed as mean ± standard deviation. The differences between two groups were analyzed by *t*-test, and one-way ANOVA analyzed the differences between multiple groups. The sample sizes of all experiments were guaranteed to be at least three, and the results were expressed as statistically significant at $p < 0.05$. $\alpha$: $p < 0.05$ vs PCL, $\alpha\alpha$: $p < 0.01$ vs PCL, $\alpha\alpha\alpha$: $p < 0.001$ vs PCL, $\alpha\alpha\alpha\alpha$: $p < 0.0001$ vs PCL, $\beta$: $p < 0.05$ vs OSP/PCL, $\beta\beta$: $p < 0.01$ vs OSP/PCL, and $\beta\beta\beta$: $p < 0.001$ vs OSP/PCL.

## 3. RESULTS

**3.1. Observation of Psoralen Nanospheres and OSP under SEM.** As depicted in Figure 1A, the microspheres exhibited a uniform spherical morphology with excellent dispersibility, characterized by an average size of approximately 100 nm. A closer examination in Figure 1A(b) revealed the surface characteristics of the microspheres, where a subset presented a relatively smooth surface texture, while others displayed a less smooth appearance, potentially due to minor aggregation phenomena. Figure 1B(a) illustrates the oyster shell powder particles, which manifested as irregularly shaped and sized granules and flakes, indicative of a polycrystalline nature. The presence of smaller particles and fragments in the image (Figure 1B(b)) suggested that the oyster shell powder underwent mechanical compression during its preparation, resulting in a heterogeneous distribution of particle sizes.

**3.2. Characterization of Composite 3D Scaffolds.** *3.2.1. Topographic Observation.* As shown in Figure 2A, the scaffolds were successfully prepared by a 3D printing extrusion molding system. The PCL scaffold and the PCL scaffold containing 5% oyster shell powder have smooth and

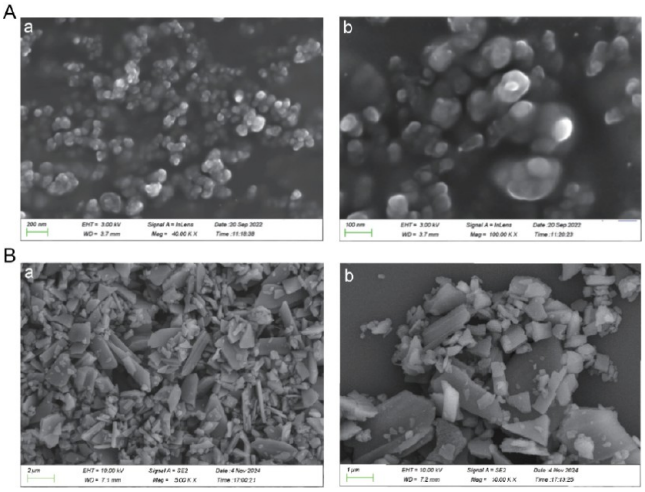


**Figure 1.** SEM of psoralen nanospheres and OSP. (A) Nanosphere images at (a) $4 \times 10^4\times$ and (b) $1 \times 10^5\times$ and (B) OSP images at (a) $5 \times 10^3\times$ and (b) $1 \times 10^4\times$.

flat white surfaces. Both scaffolds look roughly the same, except that the hybrid scaffold is whiter in color, which is considered to be due to the addition of oyster shell powder. These scaffolds contain many interconnected square- or rhombus-shaped pores with a pore diameter of about 250 $\mu$m, which facilitate the exchange of substances and the discharge of metabolic wastes, and they are conducive to the growth of newborn bone tissues,[20] so as to provide a suitable structure for cell growth.

*3.2.2. Porosity.* As shown in Figure 2B, the porosities of pure PCL and 5%OSP/PCL scaffolds were measured to be (28.86 ± 1.03)% and (25.95 ± 8.73)%, respectively. There was no significant difference in comparing the two kinds of scaffolds' porosity ($p > 0.05$), which shows that the incorporation of oyster shell powder did not significantly affect the scaffolds' porosity.

*3.2.3. Measurement of Mechanical Properties.* Figure 2C shows the stress−strain curves of pure PCL and the 5%OSP/PCL scaffolds. The modulus of elasticity is calculated as $E = \varepsilon/\sigma$, $E$ denotes the elasticity modulus, $\sigma$ denotes the stress (force per unit area), and $\varepsilon$ denotes the strain (ratio of length change to original length). The elastic modulus of pure PCL scaffolds was (31.73 ± 2.05) MPa, while that of 5%OSP/PCL scaffolds was (11.24 ± 2.84) MPa. The difference between the two groups was significant ($p < 0.0001$), which may be attributed to the fact that the 5%OSP/PCL scaffolds showed microscopic cracks due to the incorporation of oyster shell powder, and the mechanical strength was lower than that of the pure PCL scaffolds. Still, the mechanical properties of both scaffolds reached the level required for bone tissue engineering in terms of mechanical properties.[21]

**3.3. Adhesion of Nanospheres to the Scaffold.** The adhesion of nanospheres to the two types of scaffolds was observed by electron microscopy. The ultrastructure of pure PCL and 5%OSP/PCL scaffolds loaded with psoralen nanospheres is shown in Figure 2D. The nanospheres were seen to adhere roughly uniformly to the surface of the composite 3D scaffolds under SEM, which were tightly bonded. Some of the nanospheres underwent the phenomenon of agglomeration.

**3.4. Biocompatibility Testing of Composite Scaffolds with BMSCs.** *3.4.1. CCK-8 Cell Proliferative Activity Assay.*


https://doi.org/10.1021/acsomega.4c09221
ACS Omega 2025, 10, 2231−2242

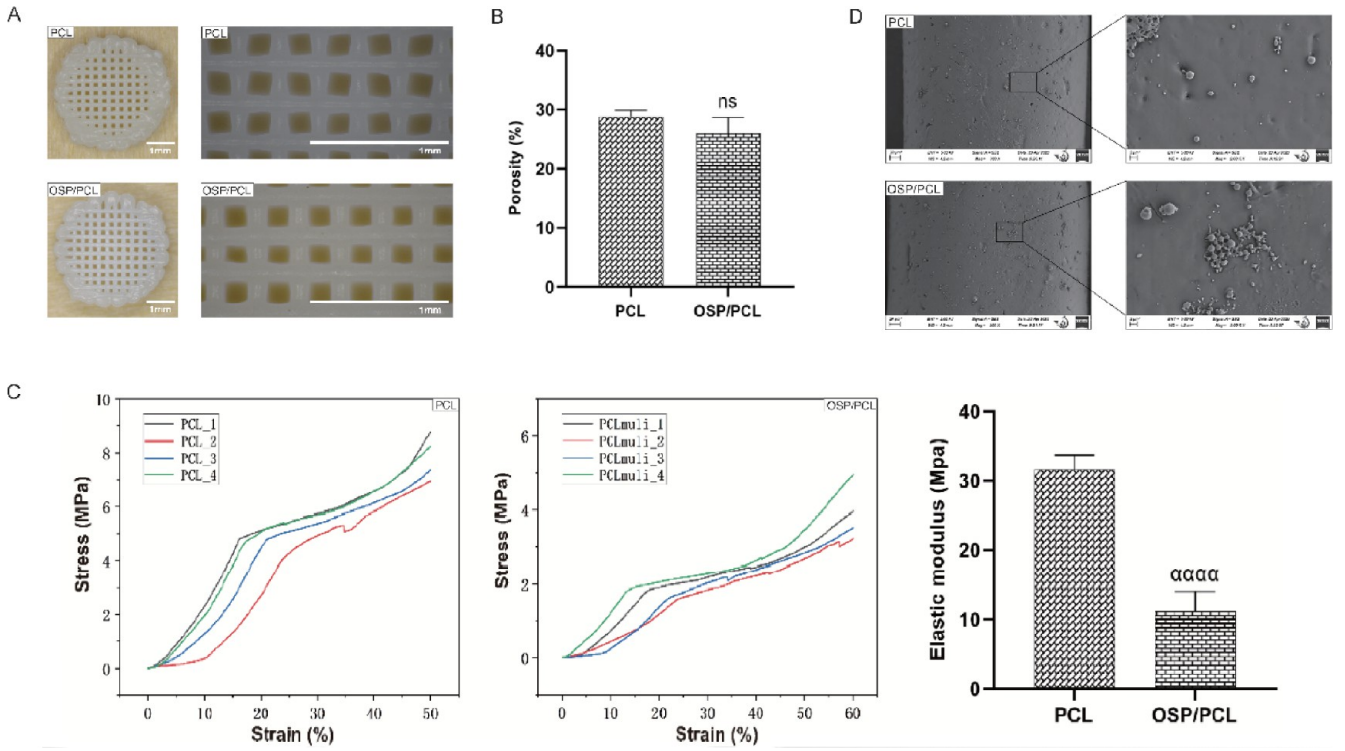


**Figure 2.** Observation of stent characterization and nanosphere adhesion. (A) Scaffold appearance and localized magnified view; (B) comparative analysis of the porosity of the two scaffolds; (C) stress−strain curves and elastic modulus analysis of the two scaffolds ($n = 4$); and (D) adhesion of scaffolds to nanospheres observed under SEM; data were shown as mean ± SD, ns: $p > 0.05$ vs PCL, $\alpha\alpha\alpha\alpha$: $p < 0.0001$ vs PCL.

Figure 3 shows no significant difference in cell proliferation rate between the groups of scaffolds, PCL scaffolds, 5%OSP/PCL scaffolds, and psoralen + 5%OSP/PCL scaffolds on day 1. However, on day 4, the proliferation rates of the PCL scaffold, 5%OSP/PCL scaffold, and psoralen + 5%OSP/PCL scaffold groups were 1.737 ± 0.01, 1.868 ± 0.05, and 2.220 ± 0.04 (×100%), respectively, and the cell proliferation rate of the psoralen + 5%OSP/95% scaffold group was significantly higher than that of the PCL scaffold group ($p < 0.01$) and 5%OSP + PCL95% group ($p < 0.05$), indicating that the psoralen + 5% OSP/PCL scaffold could promote the proliferation of BMSCs. On day 7, there was no significant difference in the cell proliferation rate among the groups, indicating that all three groups of scaffolds had good biocompatibility for BMSCs.

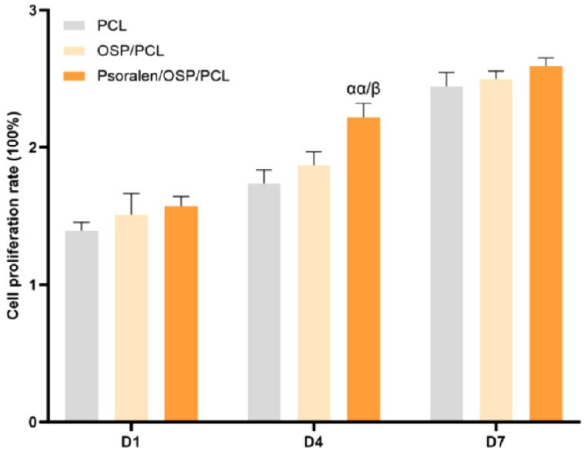


**Figure 3.** Cell proliferative activity assay of three groups of scaffolds on days 1, 4, and 7. Data were shown as mean ± SD, $\alpha\alpha$: $p < 0.01$ vs PCL, $\beta$: $p < 0.05$ vs OSP/PCL.

*3.4.2. Cell Live−Dead Assay.* Cell live−dead experiments were performed on days 1 and 3 of the coculture of BMSCs with the scaffolds to detect the biocompatibility of the scaffolds with the cells in each group. Figure 4A shows the cell live−dead staining results of the three groups of scaffolds and BMSCs compliant with the first and third day of culture. From the figure, it can be observed that the number of live cells was significantly lower in the PCL group. There were substantially more live cells on the surface of the psoralen + 5%OSP/PCL scaffolds than in the PCL group, and the levels of psoralen + 5%OSP/PCL scaffolds were significantly higher than those of the scaffolds in the 5%OSP/PCL group, suggesting that the incorporation of psoralen facilitated cell survival. According to ImageJ image processing statistics, as shown in Figure 4B, the number of live cells on psoralen + 5%OSP/PCL scaffolds is higher than that of other groups on day 1 and day 4, which was statistically significant.

*3.4.3. ALP Staining and Quantitative Analysis.* As shown in Figure 5A, 40× and 100× microscopy images showed that the cell viability on all three groups of scaffolds was good. Still, the number of cells adhering to the PCL group, 5%OSP/PCL scaffolds, was relatively less than that of the psoralen + 5% OSP/PCL scaffolds. Cellular ALP expression was quantitatively analyzed on days 4 and 7 of the composite culture. As shown in Figure 5B, ALP expression was significantly higher in the 5%OSP/PCL scaffolds and the psoralen + 5%OSP/PCL scaffolds than in the PCL scaffolds on days 4 and 7 ($p < 0.001$ and $p < 0.001$, respectively). At the same time, the psoralen + 5%OSP/PCL scaffolds had a higher ALP expression level significantly higher in the psoralen + 5%OSP/PCL scaffold


https://doi.org/10.1021/acsomega.4c09221
ACS Omega 2025, 10, 2231−2242

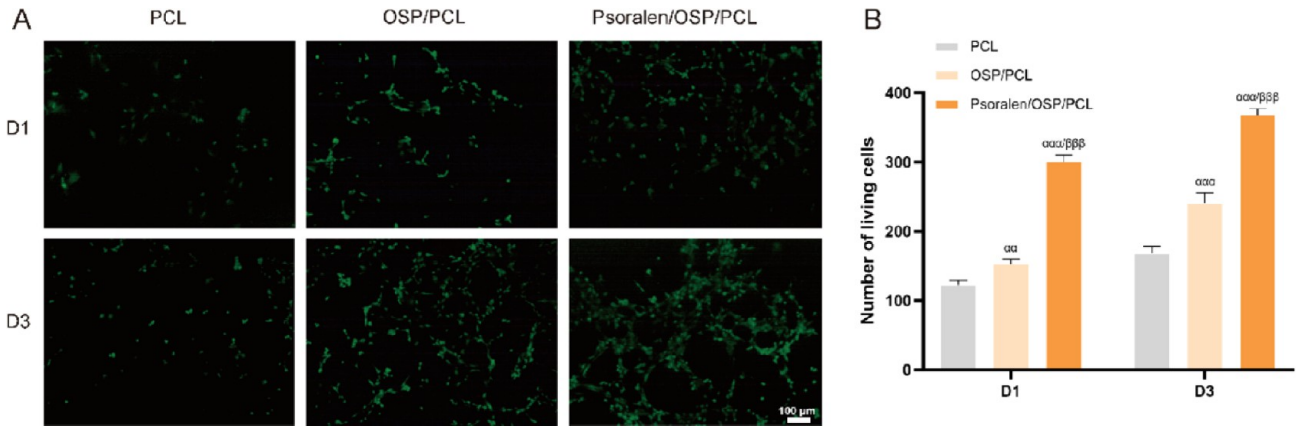


**Figure 4.** Cell viability and death assay of three sets of scaffolds with BMSCs conformed to culture on days 1 and 3. (A) Fluorescence microscopic observation of cell live−dead staining results and (B) quantitative analysis of live cells on the scaffolds in each group on days 1 and 3. Data were shown as mean ± SD, *αα*: $p < 0.01$ vs PCL, *ααα*: $p < 0.001$ vs PCL, *βββ*: $p < 0.001$ vs OSP/PCL.

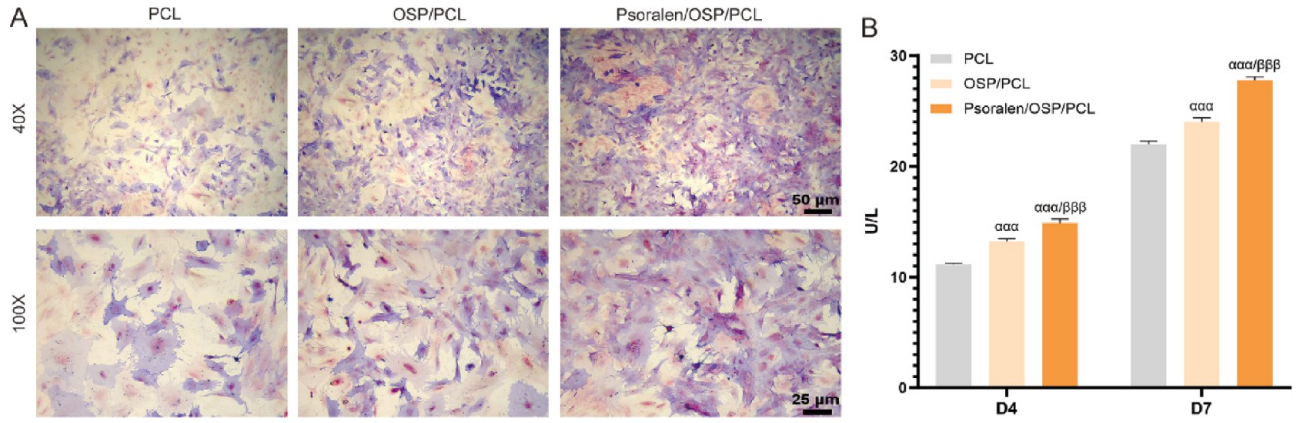


**Figure 5.** ALP staining of cells after 4 days of complex culture and quantitative analysis of cellular ALP expression on days 4 and 7. (A) Cellular ALP staining results under different magnification (40×, 100×) of optical microscope on day 4 of cell-scaffold composite culture and (B) quantitative analysis of cellular ALP expression on days 4 and 7. Data were shown as mean ± SD, *ααα*: $p < 0.01$ vs PCL, *βββ*: $p < 0.01$ vs OSP/PCL.

than in the 5%OSP/PCL scaffold ($p < 0.001$ and $p < 0.001$, respectively).

*3.4.4. Scanning Electron Microscopy Observation of Adhesion of BMSCs to Composite Scaffolds.* As shown in Figure 6, in the scanning electron microscopy observation on day 3 of the composite culture, adherent BMSCs (in red circle) appeared on the surface and near the microtiter holes of PCL scaffolds, 5%OSP/PCL scaffolds, and psoralen + 5%OSP/PCL scaffolds in the form of a three-dimensional long pike, and psoralen + 5%OSP/PCL scaffolds had the most cellular adherence and the best cell morphology. The dehydration, fixation, and other operations during the preparation stage for SEM might lead to the different shapes of cells.

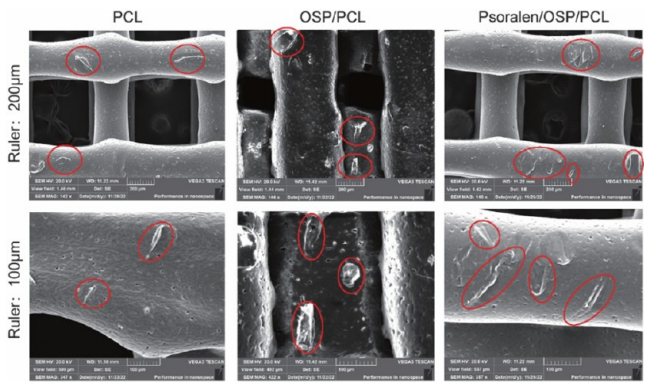


**Figure 6.** Observation of three groups of scaffolds in a complex culture with BMSCs under SEM. BMSCs were circled in red.

**3.5. Evaluation of the Efficacy of Composite Scaffolds for Repairing Cranial Defects in Rats.** *3.5.1. Bone Defect Model Preparation and Scaffold Filling.* The diameter of the defect was 5 mm, the edge was flat and smooth, the periosteum was removed thoroughly, the scaffold material and the defect were well embedded, and the rats were kept warm after the layered suture to recover naturally (Figure 7). Penicillin was injected intramuscularly for three consecutive days, and erythromycin ointment was coated in the defect's wound to prevent infection. Two rats in each group died, and eight rats survived due to improper operation of the modeling process and postoperative infection.

*3.5.2. In Vivo Toxicity Analysis of Composite Scaffolds.* The main metabolic organs of rats in each group were stained with H−E in the second week after the completion of modeling, and the *in vivo* toxicity of each scaffold was determined by observing its histological morphology. As shown in Figure 8, apparent abnormalities were found in the



https://doi.org/10.1021/acsomega.4c09221
ACS Omega 2025, 10, 2231−2242

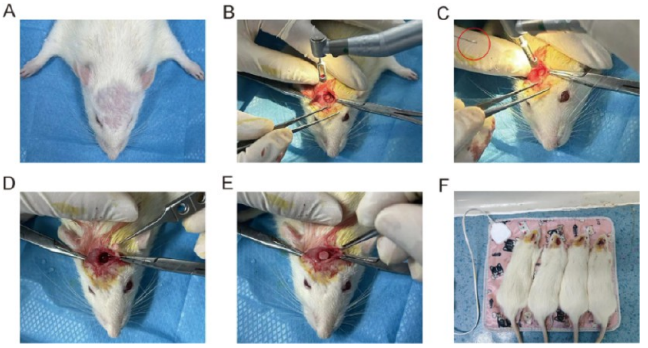


**Figure 7.** Process of preparation and scaffold filling in the rat cranial defect model. (A) After the rats entered the anesthesia state, the skin was prepared and the prone position was taken on the middle sheet; (B) the whole cranium was removed by using a ring drill with a diameter of 5 mm; (C) 0.9% saline was dripped to cool down the temperature during the whole process of drilling and removing the cranium; (D) the cranial bone fragments were taken out; (E) corresponding scaffolds were implanted according to different subgroups; and (F) the trauma was closed and kept warm, and the rats were allowed to wake up naturally.

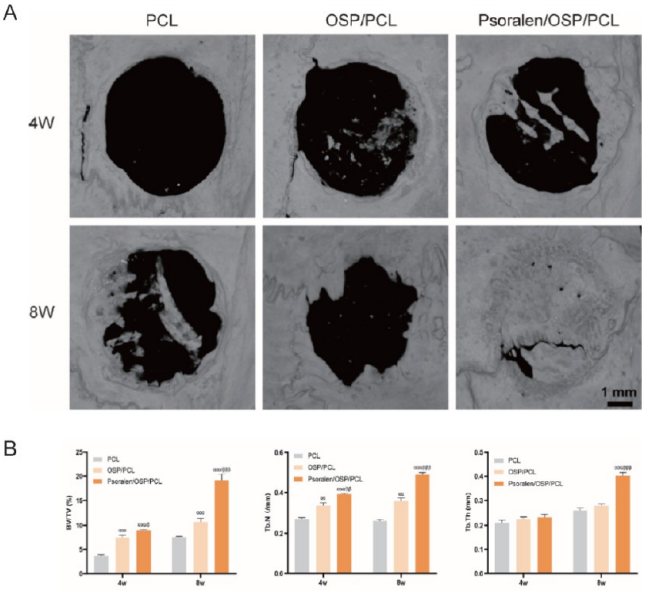


**Figure 9.** (A) 3D reconstruction of cranial micro CT and (B) analysis of different groups of rats. Data were shown as mean ± SD, $\alpha\alpha$: $p < 0.01$ vs PCL, $\alpha\alpha\alpha$: $p < 0.01$ vs PCL, $\beta$: $p < 0.05$ vs OSP/PCL, $\beta\beta$: $p < 0.01$ vs OSP/PCL, $\beta\beta\beta$: $p < 0.01$ vs OSP/PCL.

liver, spleen, kidney, and heart of the rats in each group under the light microscope, suggesting that there was no obvious *in vivo* toxicity of the PCL scaffolds, 5%OSP/PCL scaffolds, and psoralen + 5%OSP/PCL scaffolds in the three groups of scaffolds.

*3.5.3. Micro CT.* Micro CT was performed on the rats at weeks 4 and 8 after the completion of modeling to observe the local bone defect repair.

Figure 9A shows each group's micro CT 3D modeling maps of rat skulls. As can be seen from the figure, the newborn cranial bone area showed an increasing trend among the PCL group, 5%OSP/PCL scaffold, and psoralen + 5%OSP/PCL scaffold in both week 4 and week 8, which corresponded to the above statistical analysis, indicating that the psoralen + 5% OSP/PCL scaffold had a good effect in repairing the critical bone defect repair in rats.

As shown in Figure 9B, a histogram of the calculated BV/TV, it can be seen that the BV/TV values of the crania in each group gradually increased from 4 to 8 weeks. The psoralen + 5%OSP/PCL scaffolds and the 5%OSP/PCL group scaffolds increased significantly more than the PCL scaffolds ($p < 0.001$ and $p < 0.001$, respectively), whereas psoralen + 5%OSP/PCL scaffolds had a higher BV/TV level than the 5%OSP/PCL scaffold ($p < 0.05$). This elevation was even more significant at week 8 ($p < 0.001$). The results of Tb.Th showed that there was no significant difference between the groups at week 4 ($p > 0.05$), which was not statistically significant, whereas the psoralen + 5%OSP/PCL scaffold was significantly higher than that of the other two groups at week 8 ($p < 0.001$ *vs* $p < 0.001$), which was statistically significant. The above results suggest that the addition of psoralen promotes new bone formation in the repair of critical bone defects in rats.

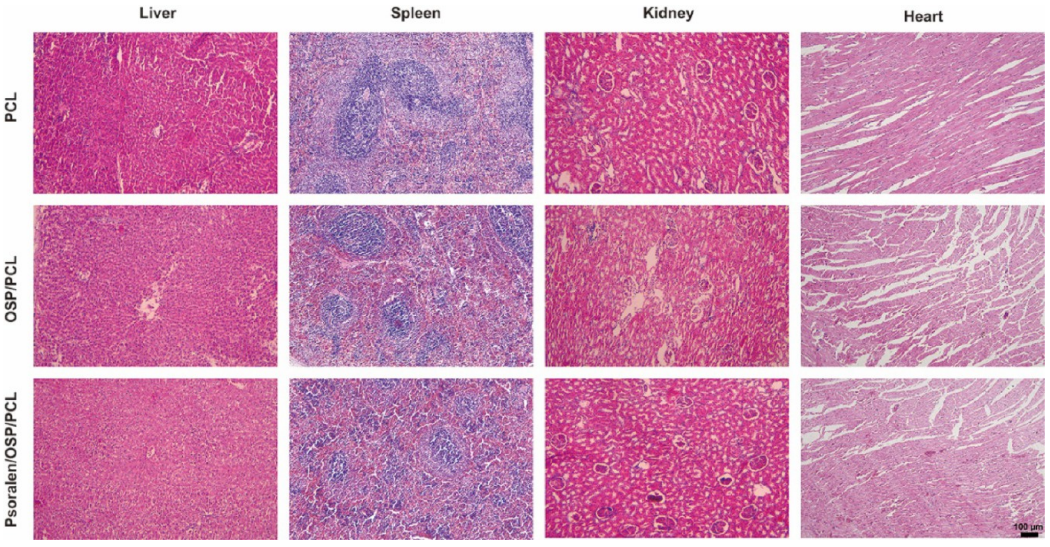


**Figure 8.** In vivo toxicity analysis of different scaffolds.



https://doi.org/10.1021/acsomega.4c09221
ACS Omega 2025, 10, 2231−2242

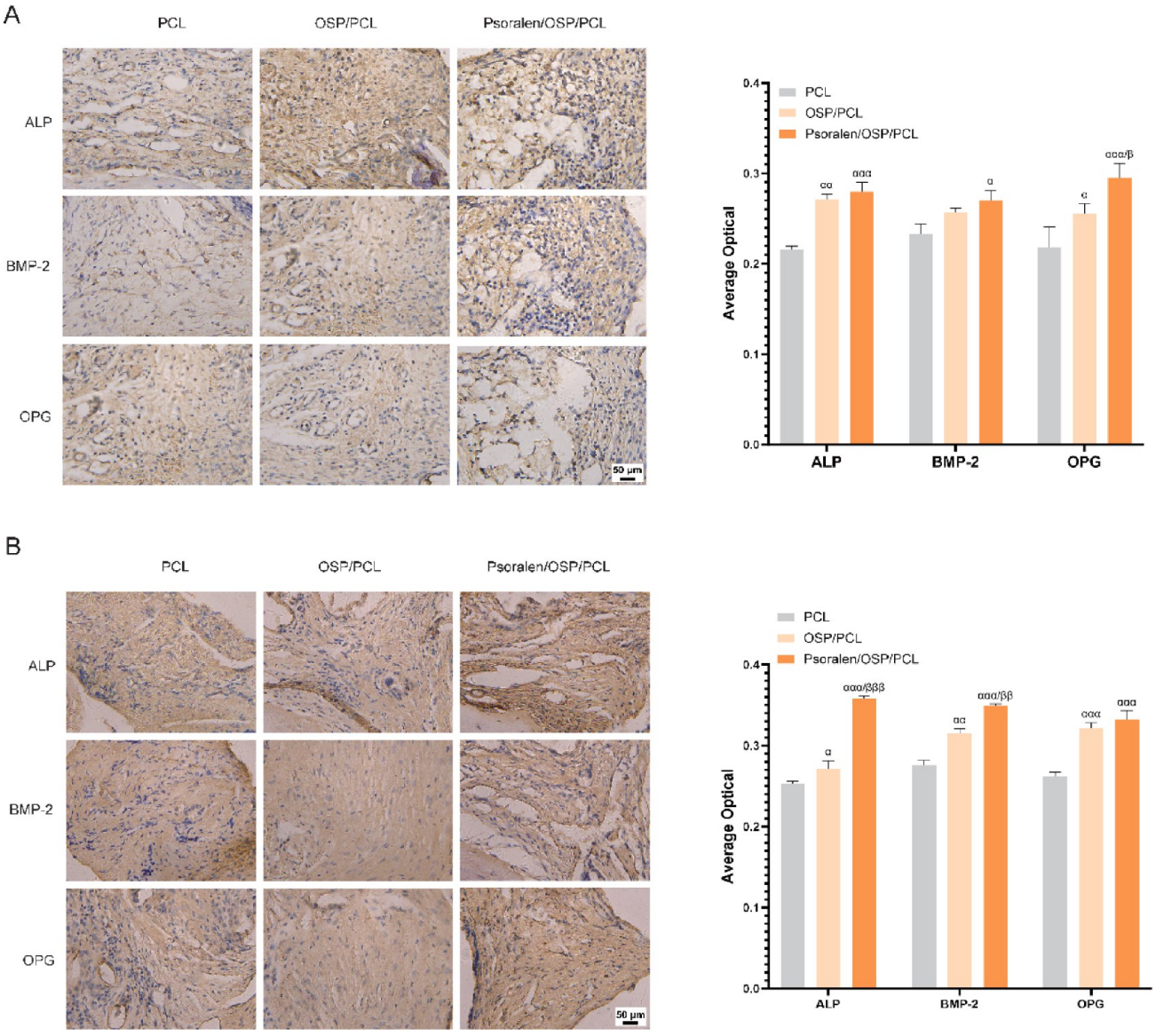


**Figure 10.** Immunohistochemical staining analysis of bone defect sites in each group at 4 and 8 weeks postoperatively. (A) Immunohistochemical images and quantitative analysis of ALP, BMP-2, and OPG antibodies at the bone defect site in each group at 4 weeks postoperatively and; (B) immunohistochemical images and quantitative analysis of ALP, BMP-2, and OPG antibodies at the bone defect site in each group at 8 weeks postoperatively. Data were shown as mean ± SD, $\alpha$: $p < 0.05$ vs PCL, $\alpha\alpha$: $p < 0.01$ vs PCL, $\alpha\alpha\alpha$: $p < 0.001$ vs PCL, $\beta$: $p < 0.05$ vs OSP/PCL, $\beta\beta$: $p < 0.01$ vs OSP/PCL, $\beta\beta\beta$: $p < 0.001$ vs OSP/PCL.

*3.5.4. Histologic Staining of Bone Regeneration at the Scaffold Site.* ALP, BMP-2, and OPG immunohistochemistry were performed in the defect area at 4 and 8 weeks after surgery, respectively. ALP is an essential marker of osteoblast differentiation and maturation, and its activity can reflect the differentiation and functional status of the osteoblasts. BMP-2 has the effect of inducing osteoblasts to proliferate and differentiate, and it can promote fracture healing. OPG mainly affects bone metabolism, inhibits osteoclast differentiation, promotes apoptosis of mature osteoclasts, and belongs to bone formation markers. Figure 10A shows the immunohistochemical results of rat skulls in each group at week 4. ALP expression was significantly increased in 5%OSP/PCL scaffolds and psoralen + 5%OSP/PCL scaffolds compared with that of PCL scaffolds ($p < 0.01$ and $p < 0.001$, respectively); BMP-2 expression was elevated in psoralen + 5%OSP/PCL scaffolds compared with PCL scaffolds ($p < 0.05$); 5%OSP/PCL scaffolds had elevated expression ($p < 0.05$); and 5%OSP/PCL scaffolds showed improved expression ($p < 0.05$); the OPG expression levels of both 5%OSP/PCL scaffold and psoralen + 5%OSP/PCL scaffold were elevated compared with the PCL group ($p < 0.05$ and $p < 0.001$), and the elevation of psoralen + 5%OSP/PCL scaffold was more pronounced than that of 5% OSP/PCL scaffold ($p < 0.05$).

The immunohistochemical results of rat skulls in each group at week 8 are shown in Figure 10B. The elevated ALP expression of psoralen + 5%OSP/PCL scaffolds and 5%OSP/PCL scaffolds was higher than that of PCL scaffolds ($p < 0.001$ and $p < 0.05$), respectively, and the ALP expression of psoralen + 5%OSP/PCL scaffolds compared to scaffolds of 5%OSP/PCL group was more significant ($p < 0.001$); the trend of BMP-2 expression was similar to that of ALP between the groups, and it is noteworthy that it was significantly higher in the 5%OSP/PCL scaffold compared with the PCL scaffold ($p$


https://doi.org/10.1021/acsomega.4c09221
ACS Omega 2025, 10, 2231−2242

< 0.01); the difference in the effect of OPG expression between the psoralen + 5%OSP/PCL scaffold and the 5% OSP/PCL scaffold was not significant ($p > 0.05$). Still, both had significant elevation compared with the PCL scaffold ($p < 0.001$ and $p < 0.001$).

The above results were consistent with the results of micro CT, suggesting that both the psoralen + 5%OSP/PCL scaffold and 5%OSP/PCL scaffold could enhance bone formation-related proteins, and both were effective in repairing bone defects, among which the psoralen + 5%OSP/PCL scaffold was the most effective in repairing bone defects.

## 4. DISCUSSION

**4.1. Composite Bone Tissue Engineering Materials Are Preferred for Large Bone Defects.** 3D printing is a new technology that has emerged in recent years and is now widely used in many disciplines, such as bone and joint, craniomaxillofacial, spinal, and hand and foot surgery.[22,23] 3D printing for bone tissue engineering scaffolds and their repair of bone tissue defects is also a current research hotspot both domestically and internationally.[24,25] The construction of artificial bone materials is mainly studied from three aspects: physical and chemical structure, chemical properties, and biological activity of the scaffold. In response to diverse clinical bone injuries and the complex and changing *in vivo* environment, it is difficult for a single material to meet the requirements of various aspects of bone tissue engineering. In contrast, composite scaffold materials have good biocompatibility and bone tissue repair ability, which can genuinely realize the *in vivo* reconstruction of bone tissues. It is a promising bone tissue engineering scaffold for application.[26,27] For example, nanohydroxyapatite coatings adhered to titanium scaffolds can interact with the extracellular matrix to promote bone repair.[28] Two biodegradable biomaterials, calcium phosphate ceramics and polylactic acid, are widely used in clinical practice; the former has good bioactivity and affinity but brittle and low bending strength, and the latter is a polymer that can be degraded over an extended period in the body. Its biological properties are also different; the composite of the two has a perfect complementary effect and is a new scaffold material for bone tissue engineering.[29]

**4.2. Psoralen + 5%OSP/PCL Scaffold Effectively Promotes BMSCs Differentiation In Vitro.** The structural characteristics of the scaffold itself are vital aspects of bone tissue engineering. Good biocompatibility, excellent mechanical properties, and osteoinductivity are three necessary conditions that an ideal scaffold system should possess.[30] The SEM images of psoralen nanospheres (Figure 1A) indicate that the uniform spherical shape and appropriate size may contribute to the stability and biocompatibility of microspheres in biological systems and may also affect their accumulation and release properties at the target site. The irregular particle morphology and rough surface of the OSP may have increased the specific surface area of oyster shell powder, thus improving its potential for adsorption, catalysis, and other applications (Figure 1B). Through computer-aided design, we prepared PCL scaffolds with multidimensional porosity with 5%OSP/PCL scaffolds using 3D printing technology, which was observed on an electron microscope with a regular pore structure, and each pore was connected, and the mechanical test verified that it had good mechanical properties. BMSCs have a strong renewal capacity and high differentiation potential. They can develop into multiple types of osteoblasts under certain conditions, which are key to maintaining standard bone structure in the bone marrow. They have been a popular cell type selected for 3D bioprinting for bone repair.[31] Studies have shown that BMSCs can accelerate the maturation and ossification of osteoporotic fracture scabs to help restore the mechanical properties of bones, and their unique physiological properties can be applied to cartilage tissue engineering to compensate for the limited self-repairing ability of cartilage lesions and osteoarthritis.[32] BMSCs have the characteristics of easy access to materials, strong proliferative force, ease of culture *in vitro*, etc. Under certain conditions, they can be induced to differentiate into the desired tissue cells by the monomers of traditional Chinese medicines, such as psoralen, astragali methyl glycoside, and ginseng saponin.[33] We constructed a cell-scaffold coculture system and found that PCL scaffolds, 5%OSP/PCL scaffolds, and psoralen + 5% OSP/PCL scaffolds had no significant toxicity to BMSCs by CCK-8 cytotoxicity and proliferative activity assay. We found that BMSCs cells could adhere, stretch, and stick well on the surface of the scaffolds by scanning electron microscopy, and finally, by ALP assay, it was found that both 5%OSP/PCL scaffold and psoralen + 5%OSP/PCL scaffold induced elevated ALP expression, and the latter was more robust than the former. The above results demonstrated that the psoralen + 5% OSP/PCL scaffold was effective in inducing the differentiation of BMSCs *in vitro*.

**4.3. Psoralen + 5%OSP/PCL Scaffold Is Effective in Repairing Cranial Defects In Vivo.** Cranial critical defects are one of the most clinically used animal models of bone defects, and the rat cranium is more amenable to surgery and reproducible but has a poor self-repairing ability and a marked dependence on osteogenesis. SD rats are easy to feed, grow faster, and can adapt to the environment; therefore, we used the SD rat cranial critical point defect model for the biological evaluation of composite scaffolds for *in vivo* bone repair. Studies related to cranial defects in rats have shown that when the diameter of the critical cranial defect is 5 mm, the defect cannot cross the sagittal suture of the rat skull, thus avoiding necrosis of the venous plexus of the sagittal sinus, which in turn reduces the likelihood of the impact of the defect size on the experimental results; therefore, we chose a diameter of 5 mm as the criterion of the critical size bone defect for the present experiment.[34] H−E staining of sections of the major metabolic organs of rats in each group revealed that none of the three groups of scaffolds had significant biotoxicity. Micro CT is a new method to visualize the internal microstructure of samples in a noninvasive and precise way. It is widely used in bone-related *in vivo* tests and allows 3D reconstruction and systematic data analysis of specific sites.[35] Micro CT results 4 and 8 weeks after scaffold implantation in cranial defects showed that the 5%OSP/PCL scaffold and psoralen + 5% OSP/PCL scaffold had better osteogenesis compared with pure PCL scaffolds, and psoralen + 5%OSP/PCL scaffolds had the best osteogenic effect, suggesting that this composite system could be more effective in promoting bone repair of cranial bone defects in rats. We found that the bone formation-related proteins ALP, BMP-2, and OPG were altered in three groups of animals by immunohistochemical assay of rat skulls, in which both 5%OSP/PCL scaffolds and psoralen + 5%OSP/PCL scaffolds promoted the elevation of the expression levels of the above proteins, and psoralen + 5%OSP/PCL scaffolds promoted more effectively the bone defect healing.


https://doi.org/10.1021/acsomega.4c09221
ACS Omega 2025, 10, 2231−2242

There are the following shortcomings in this experiment: (i) some rats died during the modeling process due to improper operation (the main reason is that the depth of the drill bit is too deep when drilling the skull, damaging the brain tissue, resulting in cerebral hemorrhage, etc.), and thus, the technique of modeling the cranial bone defects needs to be further improved, especially in the control of the depth and strength of the downward drilling. (ii) In the fourth and eighth weeks after the operation, we found that the absorption and degradation of the three groups of scaffolds were relatively low, which may have a certain degree of influence on the repair of bone defects, so the degradation rate of the composite scaffold system can be further optimized by adding another degradation rate of the product, in order to facilitate the generation of new bone in the rats themselves. (iii) The repair of bone defects requires a lot of time, and although we found that the composite system had a specific effect on the healing of bone defects through sampling observation at 4 and 8 weeks after the operation, some of the bone defects were not repaired. The observation time can be extended to 12 weeks or even longer to observe the long-term repair efficacy of this scaffolding system.

## 5. CONCLUSION

This study prepared a composite scaffold of psoralen, oyster shell powder, and PCL using 3D printing and an extrusion molding system. The in vitro and in vivo experiments confirmed that this scaffold system has good mechanical properties, osteoinductivity, and biosafety. It can promote osteogenic differentiation and upregulate the expression of osteogenic-related proteins of BMSCs to encourage the repair of bone defects, which can provide a new approach for repairing large bone defects in clinical practice. It offers a new idea for the clinical repair of large bone defects.

## AUTHOR INFORMATION


### Corresponding Authors

**Wenxiong Li** − *Shaanxi University of Chinese Medicine, Xianyang 712046, China; Key Laboratory of Chronic Muscles and Bones Diseases, Xianyang 712000, China; Affiliated Hospital of Shaanxi University of Chinese Medicine, Xianyang 712000, China*; Email: liwenxiong55@163.com

**Feng Yang** − *Shaanxi University of Chinese Medicine, Xianyang 712046, China; Key Laboratory of Chronic Muscles and Bones Diseases, Xianyang 712000, China*; Email: yangfengdudu@163.com

### Authors

**Tianpeng Liu** − *Shaanxi University of Chinese Medicine, Xianyang 712046, China; Key Laboratory of Chronic Muscles and Bones Diseases, Xianyang 712000, China*; orcid.org/0009-0004-3145-3309

**Menghan Chen** − *Key Laboratory of Chronic Muscles and Bones Diseases, Xianyang 712000, China; Hospital of Traditional Chinese Medicine of Hancheng City, Weinan 712046, China*

**Yifan Zhao** − *Shaanxi University of Chinese Medicine, Xianyang 712046, China; Key Laboratory of Chronic Muscles and Bones Diseases, Xianyang 712000, China*

**Shaochuan Zhao** − *Shaanxi University of Chinese Medicine, Xianyang 712046, China; Key Laboratory of Chronic Muscles and Bones Diseases, Xianyang 712000, China*

**Chen Rui** − *Shaanxi University of Chinese Medicine, Xianyang 712046, China; Key Laboratory of Chronic Muscles and Bones Diseases, Xianyang 712000, China*

Complete contact information is available at: https://pubs.acs.org/10.1021/acsomega.4c09221


### Author Contributions

#T.L. and M.C. contributed equally to this work. Conceptualization: F.Y.; data curation: T.L., Y.Z., and W.L.; methodology: F.Y. and W.L.; formal analysis: T.L., M.C., and S.Z.; supervision: F.Y. and W.L.; writing—original draft: T.L., M.C., C.R., S.Z., and Y.Z.; writing—review and editing: F.Y. and W.L.


### Funding

This work was supported by the National Natural Science Foundation project (grant numbers 81973889 and 82474543) and the Shaanxi Provincial Department of Science and Technology General Project in the Field of Social Development (grant number 2023-YBSF-210).


### Notes

This experiment was approved by the Laboratory Animal Ethics Committee of Shaanxi University of Traditional Chinese Medicine (Ethics Approval number SUCMDL20221116002).

The authors declare no competing financial interest.

## REFERENCES


(1) Amini, A. R.; Laurencin, C. T.; Nukavarapu, S. P. Bone tissue engineering: recent advances and challenges. *Crit. Rev. Biomed. Eng.* **2012**, *40* (5), 363−408.

(2) Schmitz, J. P.; Hollinger, J. O. The critical size defect as an experimental model for craniomandibulofacial nonunions. *Clin. Orthop. Relat. Res.* **1986**, *205*, 299−308.

(3) Stevens, M. M. Biomaterials for bone tissue engineering. *Mater. Today* **2008**, *11* (5), 18−25.

(4) Crane, G. M.; Ishaug, S. L.; Mikos, A. G. Bone tissue engineering. *Nat. Med.* **1995**, *1* (12), 1322−1324.

(5) Feng, G.; Xiao, D. Current status and clinical application of bone tissue engineering research. *West. Med.* **2016**, *28* (8), 1042−1045.

(6) Xiong, W.; Yuan, L.; Qian, G.; Huang, J.; Pan, B.; Guo, L.; Zeng, Z. Application of traditional Chinese medicine "tonifying the kidney and strengthening the bone" to bone tissue engineering scaffolds for repairing segmental bone defects. *Chin. Tissue Eng. Res.* **2023**, *27* (21), 3438−3444.

(7) Liu, W.; Li, T.; Zhang, T.; Wang, Q.; Chen, Y.; Su, X. Modification and adsorption properties of calcium in oyster shells. *Mater. Guide* **2012**, *26* (18), 88−92.

(8) Yue, S. *Preparation of oyster shell tissue-engineered bone materials and experimental study of Rab5 in osteogenic differentiation*, NIH, 2016.

(9) Mount, A. S.; Wheeler, A. P.; Paradkar, R. P.; Snider, D. Hemocyte-mediated shell mineralization in the eastern oyster. *Science* **2004**, *304* (5668), 297−300.

(10) Alam, F.; Khan, G. N.; Asad, M. H. H. B. Psoralea corylifolia L: Ethnobotanical, biological, and chemical aspects: A review. *Phytother. Res.* **2018**, *32* (4), 597−615.

(11) Ren, Y.; Song, X.; Tan, L.; Guo, C.; Wang, M.; Liu, H.; Cao, Z.; Li, Y.; Peng, C. A Review of the Pharmacological Properties of Psoralen. *Front. Pharmacol.* **2020**, *11*, 571535.

(12) Zhang, T.; Han, W.; Zhao, K.; Yang, W.; Lu, X.; Jia, Y.; Qin, A.; Qian, Y. Psoralen accelerates bone fracture healing by activating both osteoclasts and osteoblasts. *Faseb J.* **2019**, *33* (4), 5399−5410.

(13) Malikmammadov, E.; Tanir, T. E.; Kiziltay, A.; Hasirci, V.; Hasirci, N. PCL and PCL-based materials in biomedical applications. *J. Biomater. Sci., Polym. Ed.* **2018**, *29* (7−9), 863−893.

(14) Carmona, V. B.; Corrêa, A. C.; Marconcini, J. M.; Mattoso, L. H. C. Properties of a Biodegradable Ternary Blend of Thermoplastic Starch (TPS), Poly(ε-Caprolactone) (PCL) and Poly(Lactic Acid) (PLA). *J. Polym. Environ.* **2015**, *23* (1), 83−89.
(15) Patrício, T.; Domingos, M.; Gloria, A.; D'Amora, U.; Coelho, J. F.; Bártolo, P. J. Fabrication and characterization of PCL and PCL/PLA scaffolds for tissue engineering. *Rapid Prototyp. J.* **2014**, *20* (2), 145−156.
(16) Jang, J. W.; Min, K. E.; Kim, C.; Wern, C.; Yi, S. PCL and DMSO2 Composites for Bio-Scaffold Materials. *Materials* **2023**, *16* (6), 2481.
(17) Huang, Y.; Liao, L.; Su, H.; Chen, X.; Jiang, T.; Liu, J.; Hou, Q. Psoralen accelerates osteogenic differentiation of human bone marrow mesenchymal stem cells by activating the TGF-β/Smad3 pathway. *Exp. Ther. Med.* **2021**, *22* (3), 940.
(18) Tang, D. Z.; Yang, F.; Yang, Z.; Huang, J.; Shi, Q.; Chen, D.; Wang, Y. J. Psoralen stimulates osteoblast differentiation through activation of BMP signaling. *Biochem. Biophys. Res. Commun.* **2011**, *405* (2), 256−261.
(19) Mohan, S.; Karunanithi, P.; Raman Murali, M.; Anwar Ayob, K.; Megala, J.; Genasan, K.; Kamarul, T.; Balaji Raghavendran, H. R. Potential Use of 3D CORAGRAF-Loaded PDGF-BB in PLGA Microsphere Seeded Mesenchymal Stromal Cells in Enhancing the Repair of Calvaria Critical-Size Bone Defect in Rat Model. *Mar. Drugs* **2022**, *20* (9), 561.
(20) Ma, X. F.; Zhang, J. Y. Development of bone tissue engineering scaffold materials. *Chin. J. Tissue Eng. Res.* **2014**, *18* (30), 4895−4899.
(21) Hollister, S. J.; Lin, C. Y.; Saito, E.; Lin, C. Y.; Schek, R. D.; Taboas, J. M.; Williams, J. M.; Partee, B.; Flanagan, C. L.; Diggs, A. Engineering craniofacial scaffolds. *Orthod. Craniofac. Res.* **2005**, *8* (3), 162−173.
(22) Pati, F.; Song, T. H.; Rijal, G.; Jang, J.; Kim, S. W.; Cho, D. W. Ornamenting 3D printed scaffolds with cell-laid extracellular matrix for bone tissue regeneration. *Biomaterials* **2015**, *37*, 230−241.
(23) Xu, N.; Wei, F.; Liu, X.; Jiang, L.; Cai, H.; Li, Z.; Yu, M.; Wu, F.; Liu, Z. Reconstruction of the Upper Cervical Spine Using a Personalized 3D-Printed Vertebral Body in an Adolescent With Ewing Sarcoma. *Spine* **2016**, *41* (1), No. E50−4.
(24) Mozdzen, L. C.; Rodgers, R.; Banks, J. M.; Bailey, R. C.; Harley, B. A. Increasing the strength and bioactivity of collagen scaffolds using customizable arrays of 3D-printed polymer fibers. *Acta Biomater.* **2016**, *33*, 25−33.
(25) Tarafder, S.; Koch, A.; Jun, Y.; Chou, C.; Awadallah, M. R.; Lee, C. H. Micro-precise spatiotemporal delivery system embedded in 3D printing for complex tissue regeneration. *Biofabrication* **2016**, *8* (2), 025003.
(26) Zhou, R.; Xu, W.; Chen, F.; Qi, C.; Lu, B. Q.; Zhang, H.; Wu, J.; Qian, Q. R.; Zhu, Y. J. Amorphous calcium phosphate nanospheres/polylactide composite coated tantalum scaffold: facile preparation, fast biomineralization and subchondral bone defect repair application. *Colloids Surf., B* **2014**, *123*, 236−245.
(27) Nitzsche, H.; Lochmann, A.; Metz, H.; Hauser, A.; Syrowatka, F.; Hempel, E.; Müller, T.; Thurn-Albrecht, T.; Mäder, K. Fabrication and characterization of a biomimetic composite scaffold for bone defect repair. *J. Biomed. Mater. Res. A* **2010**, *94A* (1), 298−307.
(28) Arcos, D.; Vallet-Regí, M. Substituted hydroxyapatite coatings of bone implants. *J. Mater. Chem. B* **2020**, *8* (9), 1781−1800.
(29) Miura, K. I.; Sumita, Y.; Kajii, F.; Tanaka, H.; Kamakura, S.; Asahina, I. First clinical application of octacalcium phosphate collagen composite on bone regeneration in maxillary sinus floor augmentation: A prospective, single-arm, open-label clinical trial. *J. Biomed. Mater. Res. B Appl. Biomater.* **2020**, *108* (1), 243−252.
(30) Bose, S.; Vahabzadeh, S.; Bandyopadhyay, A. Bone tissue engineering using 3D printing. *Mater. Today* **2013**, *16* (16−12), 496−504.
(31) Zhou, Y.; Guo, H. Magnesium-based alloy scaffolds loaded with rabbit-derived bone marrow mesenchymal stem cells to construct tissue-engineered bone composite scaffolds. *Chin. Tissue Eng. Res.* **2023**, *27* (34), 5491−5496.
(32) Souza, A. T. P.; Freitas, G. P.; Lopes, H. B.; Weffort, D.; Adolpho, L. F.; Gomes, M. P. O.; Oliveira, F. S.; Almeida, A. L. G.; Beloti, M. M.; Rosa, A. L. Mesenchymal stem cell-based therapy for osteoporotic bones: Effects of the interaction between cells from healthy and osteoporotic rats on osteoblast differentiation and bone repair. *Life Sci.* **2024**, *340*, 122463.
(33) Yang, B.; Wang, N.; Tan, R.; Wang, Q.; Gu, J. Progress of Chinese herbal medicine and its monomers on the induction and differentiation of bone marrow mesenchymal stem cells. *Chin. Herb. Med.* **2022**, *53* (24), 7915−7924.
(34) Kasper, F. K.; Young, S.; Tanahashi, K.; Barry, M. A.; Tabata, Y.; Jansen, J. A.; Mikos, A. G. Evaluation of bone regeneration by DNA release from composites of oligo(poly(ethylene glycol) fumarate) and cationized gelatin nanospheres in a critical-sized calvarial defect. *J. Biomed Mater. Res. A* **2006**, *78* (2), 335−342.
(35) Akhter, M. P.; Recker, R. R. High resolution imaging in bone tissue research-review. *Bone* **2021**, *143*, 115620.


https://doi.org/10.1021/acsomega.4c09221
*ACS Omega* 2025, 10, 2231−2242